



# Influence of substrate dimensionality on the growth mode of epitaxial 3D-bonded GeTe thin films: From 3D to 2D growth

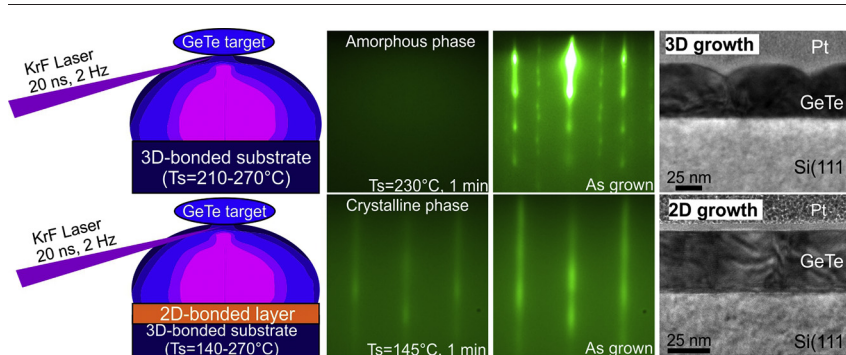
Isom Hilmi, Andriy Lotnyk\*, Jürgen W. Gerlach, Philipp Schumacher, Bernd Rauschenbach

Leibniz-Institut für Oberflächenmodifizierung e.V., Permoserstr. 15, 04318 Leipzig, Germany

## HIGHLIGHTS

- Epitaxial 3D-bonded GeTe thin films are grown by pulsed laser deposition on 3D- and 2D-bonded substrates
- Deposition on 2D-bonded substrates allows the epitaxial growth at low substrate temperatures
- A possibility of improving surface quality of epitaxial 3D-bonded thin films by employing a 2D-bonded seeding layer is shown
- Formation of overlapped twin domains with characteristic lamellar structure in HRTEM

## GRAPHICAL ABSTRACT



## ARTICLE INFO

### Article history:

Received 22 October 2018  
 Received in revised form 8 February 2019  
 Accepted 11 February 2019  
 Available online 14 February 2019

### Keywords:

Phase change materials  
 GeTe  
 2D growth  
 X-ray diffraction  
 TEM  
 Defects

## ABSTRACT

The pseudo-binary line of  $\text{Sb}_2\text{Te}_3$ -GeTe contains alloys featuring different crystalline characteristics from two-dimensionally (2D-) bonded  $\text{Sb}_2\text{Te}_3$  to three-dimensionally (3D-) bonded GeTe. Here, the growth scenario of 3D-bonded GeTe is investigated by depositing epitaxial GeTe thin films on Si(111) and  $\text{Sb}_2\text{Te}_3$ -buffered Si(111) substrates using pulsed laser deposition (PLD). GeTe thin films were grown in trigonal structure within a temperature window for epitaxial growth of 210–270 °C on unbuffered Si(111) substrates. An unconventional growth onset was characterized by the formation of a thin amorphous GeTe layer. Nonetheless, the as-grown film is found to be crystalline. Furthermore, by employing a 2D-bonded  $\text{Sb}_2\text{Te}_3$  thin film as a seeding layer on Si(111), a 2D growth of GeTe is harnessed. The epitaxial window can substantially be extended especially towards lower temperatures down to 145 °C. Additionally, the surface quality is significantly improved. The inspection of the local structure of the epitaxial films reveals the presence of a superposition of twinned domains, which is assumed to be an intrinsic feature of such thin films. This work might open a way for an improvement of an epitaxy of a 3D-bonded material on a highly-mismatched substrate (e.g. Si(111)) by employing a 2D-bonded seeding layer (e.g.  $\text{Sb}_2\text{Te}_3$ ).

© 2019 Elsevier Ltd. This is an open access article under the CC BY-NC-ND license (<http://creativecommons.org/licenses/by-nc-nd/4.0/>).

## 1. Introduction

Te-based alloys lying on the pseudo-binary line of  $\text{Sb}_2\text{Te}_3$ -GeTe are today considered as potential candidates for the next-generation non-

volatile memory media [1,2]. Recently, interesting advances have been proposed. An example is given in the concept of unique bonding mechanism owing to their crystalline phase [3,4], which further leads to a possibility of non-thermal switching mechanisms [5,6]. Another instance is in 'material tailoring' standpoint, i.e. the concept of so-called interfacial-phase change materials (iPCM), constructed out of superlattice-like structures of two different alloys [7,8], has been proven

\* Corresponding author.

E-mail address: [andriy.lotnyk@iom-leipzig.de](mailto:andriy.lotnyk@iom-leipzig.de) (A. Lotnyk).

to have significant improvements also in the switching nature. In many cases, understanding the physical background is of paramount importance to further induce many improvements on the device performance side. To this point, a fabrication of films with a higher crystalline order could provide a good platform for a deeper investigation on their physical properties including their electronic band structures, conduction mechanism as well as the switching scenario down to the atomic scale. Hence, efforts are made to grow epitaxial chalcogenide films with various methods [9–15].

One of the most interesting features of the binary line  $\text{Sb}_2\text{Te}_3$ -GeTe is the characteristics of crystalline structures spanning from  $\text{Sb}_2\text{Te}_3$  to GeTe. Residing in the end point of the binary line,  $\text{Sb}_2\text{Te}_3$  crystallizes in trigonal structure (space group  $R\bar{3}mH$ ), as depicted in Fig. 1a. The crystal is constructed out of quintuple layers (QL) stacked along the  $c$ -axis and bonded by van der Waals (vdW) type bonding. The atomic sequence along the  $c$ -axis is then -vdW gap-Te-Sb-Te-Sb-Te-. Hence,  $\text{Sb}_2\text{Te}_3$  is considered as two-dimensionally (2D) bonded material. The trigonal cell consists of three QLs with lattice constants  $a = 0.4264$  nm and  $c = 3.0455$  nm [16]. Due to this 2D-bonding nature, the growth mechanism of such layered compounds is dictated by a vdW epitaxy [17], which implies a layer-by-layer growth of thin films even on a highly mismatched Si(111) substrate grown by e.g. by pulsed laser deposition (PLD) [12].

Another endpoint of the binary line is the GeTe alloy. It exhibits a different bonding characteristic compared to that of  $\text{Sb}_2\text{Te}_3$ . GeTe also crystallizes in trigonal structure (space group  $R\bar{3}mH$ ) [18–20], with hexagonal unit cell parameters  $a = 0.4156$  nm and  $c = 1.066$  nm [18], see Fig. 1b. The structure of GeTe can also be interpreted as a rhombohedral unit cell with  $a = 0.4281$  nm and  $\alpha = 58.36^\circ$  (space group  $R\bar{3}mR$ ) [21]. The cation and anion sites are occupied by Ge and Te, respectively, with anion or cation layers stacked along [0001] according to an ABC stacking [18,21,22].

In comparison to the bonding nature of stable crystalline phases of many other alloys within the binary line like  $\text{Sb}_2\text{Te}_3$ , GeTe can be considered as a three-dimensionally (3D) bonded material. This implies a conventional ‘lattice-match epitaxy’, where the incoming adatoms are bonded to the dangling bonds of a substrate. Thus, the epitaxial quality of such thin films is dependent on the lattice mismatch to the substrate. Hence, some restrictions are encountered for the growth of epitaxial

GeTe thin films on highly-mismatched substrate materials like Si. This includes a relatively narrow epitaxial temperature window and a predominantly three-dimensional growth mode, resulting in a high surface roughness of the thin films [23,24]. The latter can be undesirable in regard of their applications.

Therefore, the main focus of this work is on the growth of 3D-bonded GeTe alloy. In the first part of the work, epitaxial GeTe films are produced on (111)-oriented Si substrates. The symmetry of (111)-oriented Si surface matches very well the symmetry of the (0001)-plane of GeTe, thus resulting in  $c$ -oriented growth of GeTe thin films. The *in-plane* lattice mismatch between the GeTe crystal and the Si (111) substrate is  $\sim 8.3\%$ , see Fig. 1b and c. In the second part, an epitaxial  $\text{Sb}_2\text{Te}_3$  thin layer was deposited on Si(111) as a seeding layer for the subsequent epitaxial growth of GeTe thin films [12,25]. The  $a$ -lattice parameter of  $\text{Sb}_2\text{Te}_3$  differs by 2.5% to that of GeTe in the trigonal lattice (or by 1% using rhombohedral settings of the unit cell) only. Since PLD growth of  $\text{Sb}_2\text{Te}_3$  on Si(111) implies a 2D growth mode [12],  $\text{Sb}_2\text{Te}_3$  material is an ideal seeding layer for the deposition of GeTe thin films. Thus, a different growth mode of GeTe on  $\text{Sb}_2\text{Te}_3$ -buffered Si(111) substrates is expected. The study of GeTe growth on such substrates is important in view of engineering of chalcogenide GeTe/ $\text{Sb}_2\text{Te}_3$ -based heterostructures for memory devices with low power consumption [7,8,26–29]. The last part of this study deals with the discussion of the local structure of epitaxial GeTe.

## 2. Experimental section

Prior to deposition, each (111)-oriented Si substrate was wet-chemically cleaned. Details of the cleaning procedure can be found in Refs. [10, 12]. Then, the substrates were heated up in vacuum to the deposition temperature  $T_s$  and kept at  $T_s$  for 30 min before the GeTe film deposition started.  $T_s$  ranged between RT and 300 °C. For the deposition of GeTe thin films, a target material with a composition close to GeTe was irradiated with 20 ns long excimer laser (KrF,  $\lambda = 248$  nm) pulses at a laser repetition rate of 2 Hz, a laser fluence of around 1 J/cm<sup>2</sup> and a number of pulses of 4000. The depositions took place in an Ar environment at an Ar partial pressure  $\sim 5 \cdot 10^{-5}$  mbar (the base pressure of the PLD system was  $\sim 5 \cdot 10^{-8}$  mbar). The Ar background gas was used in order to thermalize atoms in ablation plasma plume.

After the deposition was finished, the samples were cooled down to RT. A capping layer of amorphous  $\text{LaAlO}_x$  ( $\sim 8$  nm thick) was then deposited onto the surface of the GeTe thin films in order to minimize any possible chemical contamination and oxidation during storage in the ambient atmosphere. The composition of GeTe thin films deposited on un-reconstructed Si(111) substrates were measured by STEM-EDX to be  $\text{Ge}_{51 \pm 0.5}\text{Te}_{49 \pm 0.5}$ . The measured composition of GeTe thin film is very close to the nominal composition of the GeTe sputter target that was  $\text{Ge}_{50.1}\text{Te}_{49.9}$ .

Another set of GeTe films was deposited on Si(111) substrates covered by a thin  $\text{Sb}_2\text{Te}_3$ -seeding layer. The deposition of  $\text{Sb}_2\text{Te}_3$ -seeding layers was done at a substrate temperature of 240 °C with the number of pulses of 500 and identical PLD process parameters as aforementioned, resulting in van der Waals epitaxy of a  $\sim 4$  nm-thick layer of trigonal  $\text{Sb}_2\text{Te}_3$  [12]. The layers were subsequently cooled down to  $T_s$  (230, 210, 150 and 145 °C) for GeTe film depositions. The process parameters for the GeTe deposition are identical to those of the films deposited directly on Si(111).

Thin film growth was monitored by using an in situ reflection-high energy electron diffraction (RHEED) system. The electron beam irradiated the substrate with a small incident angle of  $2^\circ$  with respect to the surface in  $\text{Si}(1\bar{1}0)$  direction and with an acceleration voltage of 30 kV. The Si(111) substrates were kept stationary during the deposition of GeTe thin films in order to monitor in situ thin film growth process by RHEED.

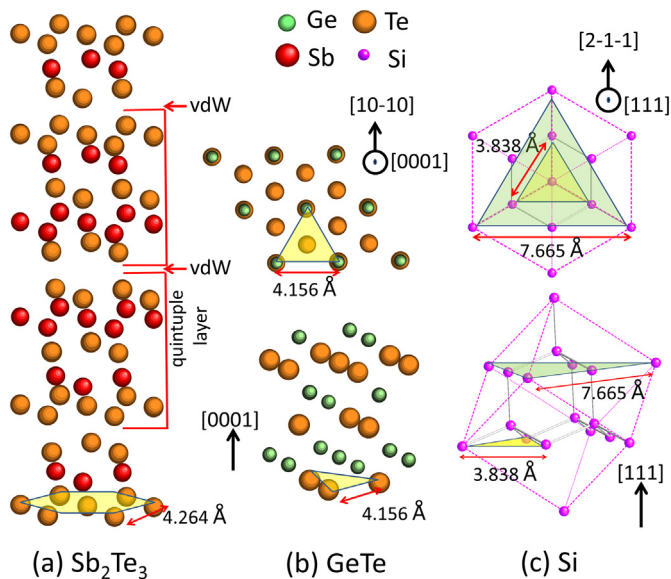


Fig. 1. Crystal structures of (a)  $\text{Sb}_2\text{Te}_3$  and (b) GeTe in trigonal cell configurations. (c) cubic Si. The transparent colored (yellow and green) hexagon and triangles mark the lattice constants of each corresponding crystal.

The structure of the thin films was studied by x-ray diffraction (XRD) using Cu  $K_{\alpha}$  radiation ( $\lambda = 0.15418$  nm) in a diffractometer with parallel beam geometry. For all XRD experiments, a graphite monochromator, mounted directly in front of the detector, was used to filter out the Cu- $K\beta$  radiation produced by the Cu target inside the X-ray tube, as well as the intense X-ray fluorescence contribution from the sample under test. All *in-plane* pole figures were measured at a Bragg angle of  $29.9^{\circ}$ . The northern pole sphere was scanned for polar angles ( $\alpha$ ) ranging from  $0$  to  $90^{\circ}$  and azimuthal angles ( $\beta$ ) ranging from  $0^{\circ}$  to  $360^{\circ}$ . The measurement window in  $2\theta$  dimension was set to  $\sim 2^{\circ}$ . The recorded intensities are plotted in stereographic projection. The thickness of thin films was determined by x-ray reflectivity (XRR) and cross-sectional scanning transmission electron microscopy (STEM). The surface topography of thin films was measured by means of atomic force microscopy (AFM) in intermittent contact mode.

Cross-sectional specimens for transmission electron microscopy (TEM) observations were prepared by a combination of focused gallium high- and argon low-energy ion beam milling [30]. The final thickness of the TEM specimens was  $30 \pm 6$  nm as measured by electron energy loss spectroscopy (EELS). The local structure of GeTe thin films was observed in a probe Cs-corrected Titan<sup>3</sup> G2 60–300 microscope operating at 300 kV accelerating voltage. For high-angle annular dark-field scanning TEM (HAADF-STEM), a probe forming annular aperture of 25 mrad was used and all images were acquired with a HAADF detector using annular ranges of 80–200 mrad, thus, fulfilling Z-contrast imaging conditions well. High-resolution TEM (HRTEM) images were recorded using a Gatan CCD camera. HRTEM image simulations were performed by using JEMS simulation package [31] whereas high-resolution HAADF-STEM micrographs were calculated using a Dr. Probe software [32]. The supercells for diffraction and Bragg reflections simulations were built up with CrystalMakerX and CaRIne Crystallography software [33].

### 3. Results and discussion

#### 3.1. Film growth

The surface properties of Si(111) substrates and the grown layer were monitored *in situ* during and after the growth of GeTe thin films using RHEED. The films grown at the substrate temperatures  $T_s$  from RT to  $190^{\circ}\text{C}$  show only a diffuse RHEED intensity pattern (not shown) during the whole deposition processes, indicating that within this temperature range the as-grown films are predominantly amorphous.

At  $T_s = 200^{\circ}\text{C}$  and higher, the growth process of GeTe thin films is different. The as-grown films show distinct RHEED patterns with no diffuse intensity, indicating that the as-deposited GeTe thin films are crystalline. The comprehensive overview of the growth modes during the deposition is presented in Fig. 2a–f, showing typical RHEED patterns of epitaxial GeTe thin films deposited on Si(111) at  $T_s$  from  $210^{\circ}\text{C}$  and above. Fig. 2a–f show important stages during the thin deposition at  $T_s = 230^{\circ}\text{C}$ . In Fig. 2a, the RHEED pattern of the (111)-oriented Si substrate is presented. A streaky pattern with Kikuchi lines is discerned, indicating a smooth surface topography and a high surface crystallinity, which is desirable for the growth of an epitaxial thin film. This further shows that the native surface oxide had been successfully removed by the wet-etch cleaning process. At the early stage of GeTe growth, a diffuse RHEED pattern was observed, as seen in Fig. 2b. Fig. 2b shows the RHEED image taken after 1 min of thin film growth. On the other hand, the RHEED pattern acquired after 1.5 min of GeTe thin film growth showed a streaky image (Fig. 2c). TEM cross-sectional analysis of GeTe thin film after 40 s of thin film growth is given in Fig. S1 (Supporting Information). The investigations showed the formation of crystalline GeTe thin islands, which were formed most probably during the cooling process. Thus, it can be concluded that the growth of epitaxial GeTe is initialized by the formation of an apparently amorphous ultra-thin GeTe layer, whereas a crystalline phase is formed after a certain period of incubation time required for GeTe crystallization. A

similar RHEED pattern for an ultra-thin GeTe film has been reported previously [34] and it was explained by an impairment in the formation of GeTe distorted structure characterized by a bonding hierarchy within the crystal [34].

As long as the deposition continued, the streaky intensity distribution becomes more intense (Fig. 2d), while the diffuse intensity gradually disappears until it completely vanishes after around 5 min. The streaky pattern indicates a smooth surface morphology of the growing layer within this deposition time duration. The streaky pattern stays without changing until around 15 min (Fig. 2e). After this period of time, a point-like (transmittance-like) intensity distribution gradually becomes more intense, indicating the occurrence of surface roughening, i.e. the growth mode turns into three-dimensional (Fig. 2f). This point-like pattern is constant until the deposition was completed. Such point-like patterns indicate large islands while the remaining streaky intensity distribution shows that the large islands are flat (this will be confirmed and discussed later on). Summarizing the RHEED investigations, the epitaxial GeTe film grows typically in 2D growth mode at the beginning of the growth, which tends to turn into 3D growth mode when the film thickness increases further. Thus, it can be stated that the pulsed laser deposited epitaxial GeTe thin film grows on Si(111) according to the Stranski-Krastanov (2D/3D) growth mode [35].

The second set of samples consists of GeTe thin films deposited on a  $\text{Sb}_2\text{Te}_3$ -seeding layer on Si(111). Fig. 2g shows the RHEED pattern of the as-deposited  $\text{Sb}_2\text{Te}_3$  thin layer. A RHEED pattern with streaky intensity distribution was present during and at the end of the  $\text{Sb}_2\text{Te}_3$  deposition, indicating the 2D growth mode of the  $\text{Sb}_2\text{Te}_3$  thin film. At the onset of GeTe thin film growth (Fig. 2h), the direct transformation from a streaky pattern of  $\text{Sb}_2\text{Te}_3$  to a streaky pattern of GeTe was observed, without a diffuse intensity distribution in the transition stage as observed with GeTe grown on Si(111). This streaky pattern is conserved until the end of the deposition (Fig. 2i), indicating a smooth surface topography of the as-grown GeTe film. Thus, in contrast to GeTe thin film grown directly on Si(111), a crystalline GeTe thin film was formed directly from the beginning of deposition process on a  $\text{Sb}_2\text{Te}_3$  seeding layer and the film growth proceeded in the Frank-van der Merwe (2D) growth mode.

The deposition rates of GeTe thin films were determined by performing XRR and STEM measurements. According to these, increasing substrate temperatures were accompanied by a decrease of deposition rates. The thickness of as-deposited amorphous films was 135 nm, resulting in the deposition rate of approximately 4 nm/min. On the other hand the thicknesses of epitaxial GeTe thin films deposited at  $210^{\circ}\text{C}$ ,  $260^{\circ}\text{C}$  and  $270^{\circ}\text{C}$  were 48 nm (1.6 nm/min), 23 nm (0.7 nm/min) and 15 nm (0.5 nm/min), respectively. Above  $T_s$  of  $270^{\circ}\text{C}$ , the rate of GeTe thin film growth was significantly minimized due to partial desorption of Ge and Te atomic species. This severe desorption at high temperature (typically around  $300^{\circ}\text{C}$ ) was also observed for epitaxial Ge-Sb-Te thin films grown on Si by PLD accompanied by a shift in chemical composition of as grown thin films [10,36].

#### 3.2. Film crystallinity and crystalline structure

The crystalline structure of GeTe thin films was investigated by measuring XRD  $2\theta/\omega$ -diffractograms. The diffractograms of all films deposited at substrate temperatures ranging from RT to  $190^{\circ}\text{C}$  do not show any Bragg reflections except those of the Si substrate (not shown). Consequently, the as-grown films are amorphous, confirming RHEED observations.

At deposition temperatures of  $200^{\circ}\text{C}$  and higher, the situation is different, which is in accordance to the RHEED observations. Fig. 3a shows XRD patterns of GeTe thin films deposited on Si(111) at  $T_s = 200, 210,$  and  $260^{\circ}\text{C}$  in red, green and orange colors, respectively. At  $T_s = 200^{\circ}\text{C}$  and higher (Fig. 3a) the patterns show mainly two intense peaks, situated at  $2\theta = 25.05^{\circ}$  and  $51.52^{\circ}$ , which are associated to the calculated (0003) and (0006) reflections of the trigonal GeTe structure (or (111) and (222) reflections, respectively, in the rhombohedral unit cell). As

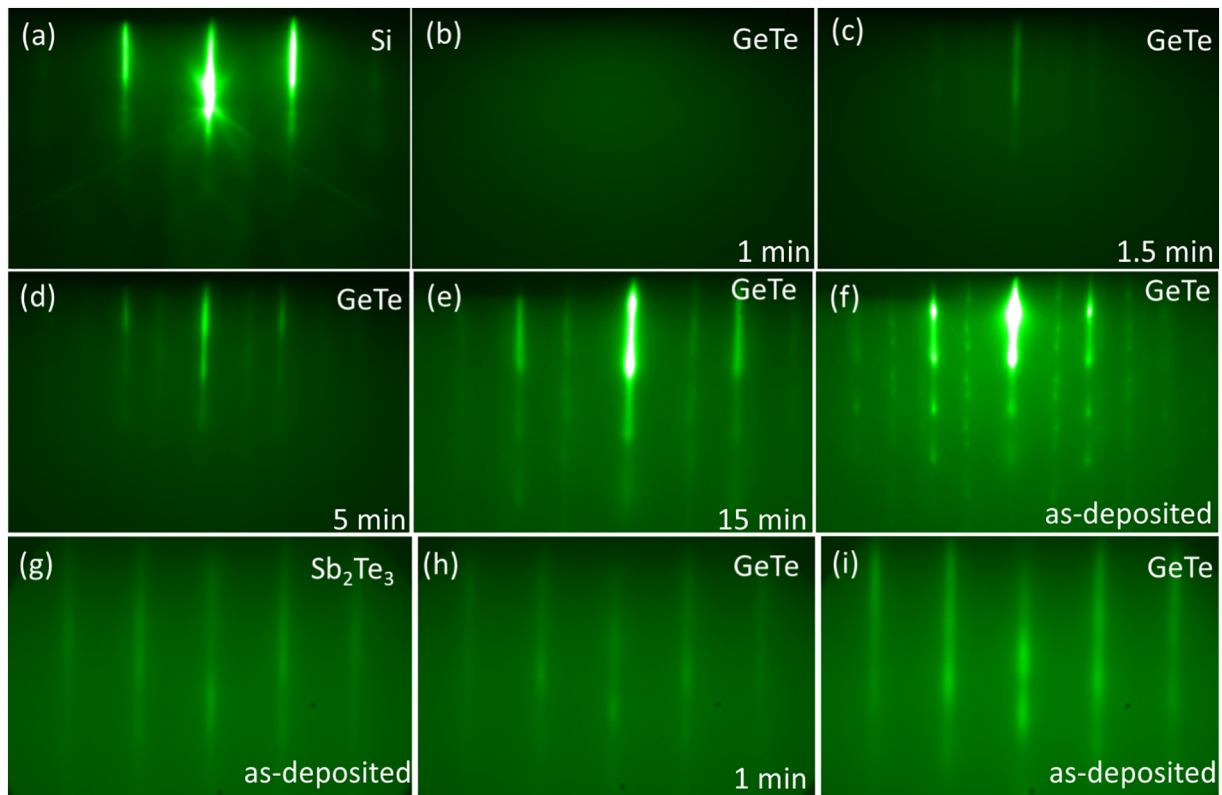


**Fig. 2.** (a) RHEED pattern of unreconstructed Si(111) surface. (b)–(f) RHEED patterns recorded in situ during deposition of GeTe at 230 °C on the Si(111) substrate. In (b) the image was taken after 1 min of thin film growth. Streaky RHEED patterns in (c) start to emanate at 1.5 min, showing a smooth surface topography. (d), (e) and (f) shows RHEED patterns of GeTe layer after 5 min and 15 min deposition process as well as after the complete deposition process, respectively. RHEED pattern in (g) gives the surface image of as-grown  $\text{Sb}_2\text{Te}_3$  thin films and the image in (h) shows a surface of GeTe layer after 1 min deposition whereas (i) gives a surface pattern of as-grown GeTe film on  $\text{Sb}_2\text{Te}_3$ -buffered Si(111) at  $T_s = 210$  °C. All RHEED patterns in (g)–(i) show a streaky intensity distribution, indicating smooth surface topographies.

only two (000 $l$ ) peaks as marked by the vertical dashed lines are present, it can be concluded that the GeTe grew exclusively with (000 $l$ ) *out-of-plane* orientation on Si(111).

The GeTe diffraction peaks, especially at higher  $2\theta$  angles (i.e. (0006) reflection), show an intensity shoulder at slightly higher  $2\theta$  values compared to the expected peak positions. This indicates the presence of reflections of oblique planes. In a previous report, this shoulder was identified to be one of the oblique GeTe  $\langle -111 \rangle$  reflections (using cubic settings) [37]. For deposition temperatures exceeding 250 °C, the double peak becomes more obvious, as represented by the film deposited at 260 °C. Identification of these double peaks was done by using the crystallographic ICSD 601273 data file. The lattice parameters of the ICSD data were modified from  $a = 0.598$  nm and  $\alpha = 88.19^\circ$  to  $a = 0.61$  nm and  $\alpha = 89.01^\circ$ , respectively. It was found that the positions of the simulated Bragg positions of (111) ( $24.84^\circ$ ) and ( $-111$ ) ( $25.42^\circ$ ) lattice planes match with the observed experimental peak positions  $24.80^\circ$  and  $25.40^\circ$  of the sample deposited at 260 °C. This confirms the co-existence of reflections of {111} oblique planes in GeTe again. Consequently, the thin film grown at 260° contains the rhombohedral GeTe phase.

In order to assess the *out-of-plane* tilt distribution of the crystallites with respect to the substrate surface, XRD  $\omega$ -scans were performed. The measurements were carried out at the example of the GeTe(0003) reflection (not shown). Films deposited at 210 °C and higher possess a typical  $\omega$ -scan full width half maximum (FWHM) of around 0.08°, indicating well-ordered *out-of-plane* (0001)-oriented films with a low mosaicity.

A set of GeTe films was also grown on a  $\text{Sb}_2\text{Te}_3$ -seeding layer on Si(111) at  $T_s = 145, 150, 210$  and 230 °C. In Fig. 3a, the  $2\theta/\omega$ -scan of a  $\text{Sb}_2\text{Te}_3$ -buffered GeTe film deposited at 150 °C is presented in blue whereas the measured Bragg reflection of epitaxial  $\text{Sb}_2\text{Te}_3$  thin film

with larger thickness is presented in black. Two reflections belonging to the (0003) and (0006) reflections of the trigonal GeTe structure can be discerned, accompanied by the set of  $c$ -plane-related Bragg reflections of the seeding layer. Since the temperature is significantly lower than the ones commonly found for epitaxial growth of GeTe on Si(111) (i.e. around 220–270 °C), this clearly demonstrates that the use of a  $\text{Sb}_2\text{Te}_3$ -seeding layer extends the epitaxial window towards lower temperatures. In addition, no splitting in Bragg reflections of GeTe structure in the whole deposition range was observed, because it is hidden by the steep flank of the  $\text{Sb}_2\text{Te}_3$  peak.

### 3.2.1. Texture analysis

For texture analysis, *in-plane* pole figure measurements were performed. Fig. 3b–d show measured GeTe{10 $\bar{1}\bar{2}$ } pole figures for selected GeTe thin films deposited at temperatures of 200, 210 and 260 °C, respectively. The pole figure of a GeTe thin film grown at a substrate temperature of 200 °C shows a predominant ring intensity distribution (Fig. 3b), indicating a fiber texture of the GeTe thin film. For the films deposited at 210 °C and 260 °C, the pole figures in Fig. 3c and d, respectively, show six pole density maxima, indicating epitaxial growth of these GeTe thin films. Each pole density maximum is situated at a polar angle  $\alpha \approx 55.3^\circ$ , corresponding to the GeTe{10 $\bar{1}\bar{2}$ } reflections, in agreement with the simulated {10 $\bar{1}\bar{2}$ } pole figure as presented in Fig. 3e. The presence of six, instead of three, pole density maxima, indicates the presence of rotation-twinned crystallites. To guide the eye, a set of pole density maxima referring to a specific oriented domain is marked by the red triangle in Fig. 3d, while the three other maxima referring to the corresponding twinned domains are marked by the dashed triangle. This twinning is commonly found in chalcogenide alloys [10,12,24,36]. Taking a closer look at both pole figures (Fig. 3c and

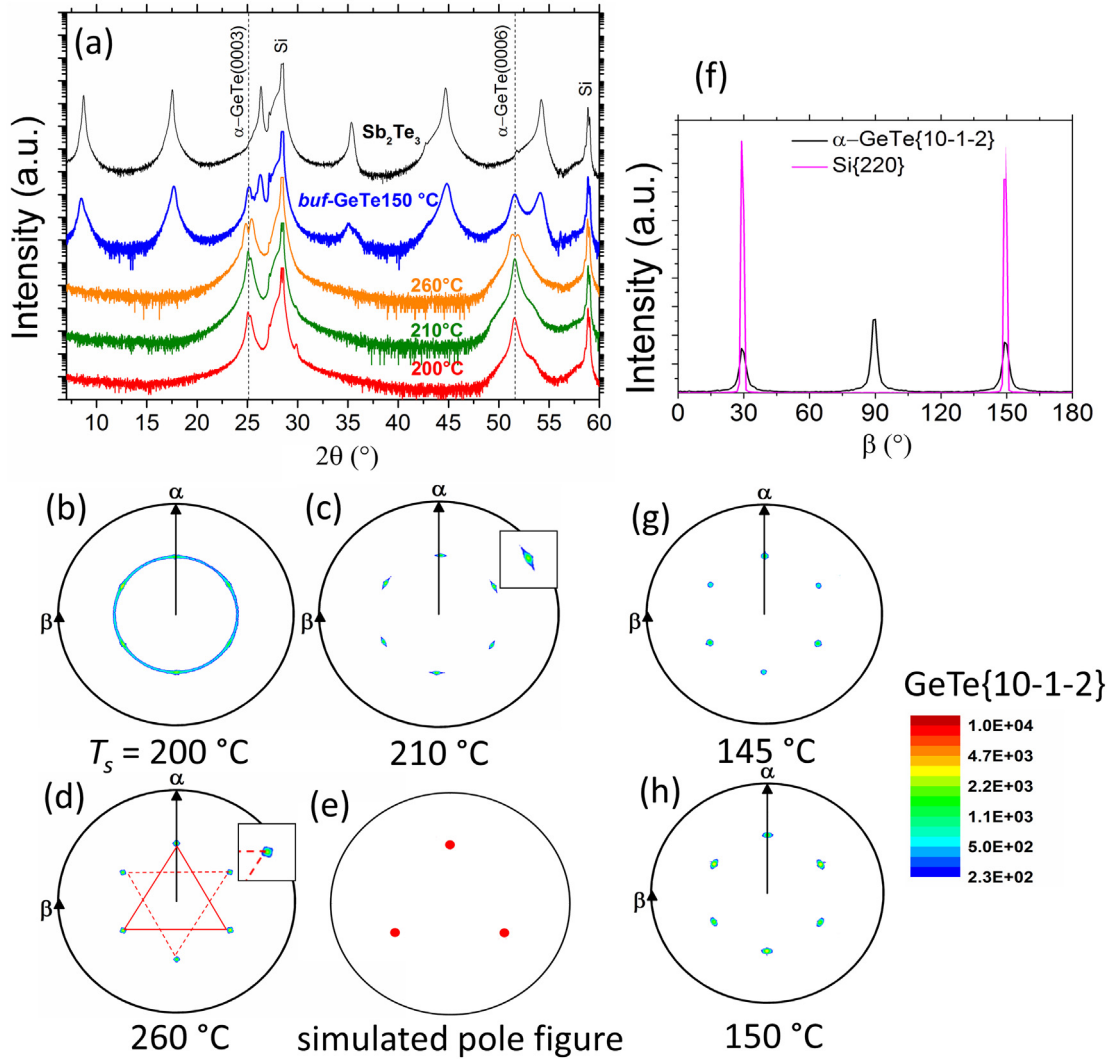


**Fig. 3.** XRD measurements of GeTe thin films: (a)  $2\theta$ -diffractograms of GeTe films deposited on unbuffered Si(111) substrate. The (0001)-oriented trigonal phase is found. Pronounced peak splitting is observed in films deposited at substrate temperature of 260 °C, indicating the formation of {111} GeTe oblique planes (see main text). The blue and black curves show the patterns of the GeTe film grown on  $\text{Sb}_2\text{Te}_3$ -buffered Si(111) substrate and of a  $\text{Sb}_2\text{Te}_3$  film [10], respectively. *In-plane* GeTe{10 $\bar{1}$ 2} ( $2\theta = 29.9^\circ$ ) pole figures of the films grown at (b) 200 °C, (c) 210 °C, (d) 260 °C, and (e) the simulated pole figure [14,30].  $\alpha$  and  $\beta$  correspond to a polar and azimuthal angle, respectively. The inserts in (c) and (d) show zoomed images of selected pole density maxima. In (f),  $\beta$  scans of GeTe{10 $\bar{1}$ 2} (black) and Si{220} (magenta) are shown. (g) and (h) show the *in-plane* pole figures of GeTe films deposited on  $\text{Sb}_2\text{Te}_3$ -buffered Si(111) substrates at 145 °C and 150 °C, respectively. The  $\theta$ - $2\theta$  is plotted in logarithmic scale whereas the  $\beta$  scan is shown in linear scale.

d), it can be discerned that the pole density maxima are somewhat narrower especially in azimuthal direction for the 260 °C film. This shows that the increase of deposition temperature within the epitaxial temperature window leads to an improvement in thin film texture.

An improvement in the epitaxial nature is shown in GeTe films grown on a  $\text{Sb}_2\text{Te}_3$ -seed layer on Si(111) substrate. The pole figures of the GeTe films grown on a  $\text{Sb}_2\text{Te}_3$ -seeding layer at 145 and 150 °C show exclusively six pole density maxima (see Fig. 3g and h), separated by an azimuthal angle of 60°. There is no ring intensity present between the maxima showing that the GeTe thin films are grown epitaxially. For the deposition of GeTe films at a temperature lower than 140 °C, the corresponding pole figures are characterized by high ring intensities showing a fiber textured thin film. The results show that by employing a  $\text{Sb}_2\text{Te}_3$ -seeding layer the activation energy for crystallization of GeTe thin films is lowered, resulting in an extended epitaxial temperature window especially towards lower temperatures down to 145 °C. A certain influence of interfaces on the device and material characteristics has been shown elsewhere [38,39]. The use of crystalline  $\text{Sb}_2\text{Te}_3$  as a template for the crystallization of amorphous GeTe was also shown to be an effective approach in lowering the activation energy for the

GeTe crystallization by 2.6 eV as well in the reduction of crystallization temperature down to 145 °C compared to the conventional crystallization temperature of GeTe of 240 °C [40,41].

In order to determine the *in-plane* epitaxial relationship of the GeTe layer to the substrate, the Si{220} pole figure was measured. Fig. 3f shows cuts extracted from the pole figures of the Si{220} (magenta) and GeTe{10 $\bar{1}$ 2} (black) reflections, i.e., intensity profiles measured as a function of the azimuthal angle  $\beta$  around the substrate [111] axis for the sample deposited at 260 °C. The  $\beta$  scan in Fig. 3f represents only single sharp peaks of GeTe, which are observed every 60° azimuthal rotation. This confirms a distinct *in-plane* orientation of the GeTe thin films. In addition, it shows that PLD deposited epitaxial GeTe thin films do not show any domain rotation around the model-calculated peaks, as commonly observed in MBE grown GeTe films on Si substrates [24]. However, the rotational domains of GeTe thin films grown by MBE were reported on (7 × 7)-reconstructed Si(111) surfaces whereas no such domains were observed on Sb passivated ( $\sqrt{3} \times \sqrt{3}$ )R30° Si(111) surfaces. In the present work the GeTe thin films were grown on unreconstructed Si(111) surfaces having mixed surface reconstruction. Moreover, the growth rates of thin films by PLD are much higher as by

MBE method, thus affecting the adatoms diffusion lengths on the substrate surface (with shorter length in the case of the PLD process and longer length in the case of the MBE growth process). These factors might influence the formation of rotation domains in PLD grown GeTe thin films.

From the  $\beta$  scans, the *in-plane* epitaxial relationship of GeTe(0001) to Si(111) can be determined to be  $\text{GeTe}[11\bar{2}0] \parallel \text{Si}[\bar{1}10]$ . Furthermore, the epitaxial relationships of the GeTe films deposited on a  $\text{Sb}_2\text{Te}_3$  seeding layer on Si was determined to be  $\text{GeTe}[11\bar{2}0] \parallel \text{Sb}_2\text{Te}_3[11\bar{2}0] \parallel \text{Si}[\bar{1}10]$ .

### 3.3. Surface morphology

The evolution of topography for each GeTe thin film deposited at different process conditions was observed by means of AFM. The film deposited at RT exhibits a smooth surface with a root mean square (RMS) roughness of 0.22 nm (not shown). Fig. 4a and b respectively show AFM images of a GeTe thin film deposited on Si(111) at  $T_s = 210^\circ\text{C}$  and its corresponding line profile drawn along the film surface, respectively. The GeTe film deposited on Si typically contains triangularly formed grains with diameters ranging between 50 and 300 nm. The triangles point out two opposite directions indicating the presence of twinned crystallites. However, some randomly orientated triangles can also be found, which indicates the presence of a small degree of domain twists in the thin film. This is in agreement with the pole figure measurement in Fig. 3c.

In the line profile of Fig. 4b, the triangular grains are separated from each other by valleys with depths of up to  $\sim 30$  nm. However, these grains possess smooth surfaces. This explains the point-like RHEED patterns coexisting with the streaky intensity distribution as observed with the as-deposited film in Fig. 2f. In other words, the point-like RHEED pattern (Fig. 2f) originates from a three-dimensional (rough) surface, while the coexisting streaky intensity originates from smooth crystallite surfaces. The determined RMS roughness is  $\sim 5$  nm. The typical RMS values of the epitaxial films deposited on Si(111) is ranging between 3 and 5 nm and is comparable with the roughness of GeTe thin films (RMS roughness  $\sim 5$  nm) produced by MBE [23].

On the contrary, GeTe thin films grown on  $\text{Sb}_2\text{Te}_3$ -buffered Si(111) substrates exhibit a higher surface quality than those deposited directly

on Si(111). Fig. 4c and d show an AFM image of a GeTe thin film deposited on a  $\text{Sb}_2\text{Te}_3$  seeding layer at  $T_s = 210^\circ\text{C}$  and its corresponding line profile marked by the red line, respectively. A smooth surface topography with an RMS value of less than 1 nm is typically obtained for GeTe films deposited on  $\text{Sb}_2\text{Te}_3$ -buffered Si(111) substrates. In Fig. 4d, a surface topography with maximum heights of 1 nm can be observed, which corresponds to a single GeTe unit cell length of  $\sim 1.07$  nm. When comparing to Fig. 4a and c, it can be concluded that an improvement of the surface quality can be achieved by employing a thin 2D grown  $\text{Sb}_2\text{Te}_3$  buffer layer. This result also reveals that by the use of a  $\text{Sb}_2\text{Te}_3$  seeding layer, the films are grown in 2D growth mode, implying a significantly smoother surface of the as-deposited film.

The microstructure of above two samples deposited at  $T_s = 210^\circ\text{C}$  on un-buffered and buffered Si(111) substrates were further studied by TEM. Fig. 4e shows a cross-sectional TEM micrograph of GeTe thin film deposited at  $210^\circ\text{C}$  on Si(111). A morphology with 3D grains separated by large valleys is visible. These grains possess smooth surfaces, as also observed by AFM. Fig. 4g shows a cross-sectional TEM image of a GeTe thin film deposited on a  $\text{Sb}_2\text{Te}_3$ -buffered Si(111) substrate. The roughness of the GeTe thin film is significantly lower compared to the film deposited on Si(111) (Fig. 4e). The surface of each grain of GeTe thin films deposited on the buffered substrates reveals ultra-smooth topology with near atomic flatness, which indicates the 2D growth mode of the GeTe thin films. A closer inspection of the microstructure of the GeTe thin films shows a wave-like contrast in bright-field TEM images (Fig. 4e and g). This reveals the presence of lattice strain in the GeTe film which is due to overlapping twin domains (see more details below). This data again demonstrates that in this case  $\text{Sb}_2\text{Te}_3$  as a seeding layer can improve the surface morphology of 3D bonded GeTe films.

### 3.4. Real structure

The local structure of GeTe thin films was investigated by high-resolution TEM and STEM. Fig. 5a shows a HRTEM image of a GeTe thin film grown on a  $\text{Sb}_2\text{Te}_3$ -buffered Si(111) substrate. The two parallel white dashed lines mark the  $\text{Sb}_2\text{Te}_3$  seeding layer with thickness of 4 nm. The GeTe grains show two distinct types of diffraction contrast. Different areas within the film are marked by b, c, and d. The corresponding structural information of the areas obtained by fast Fourier

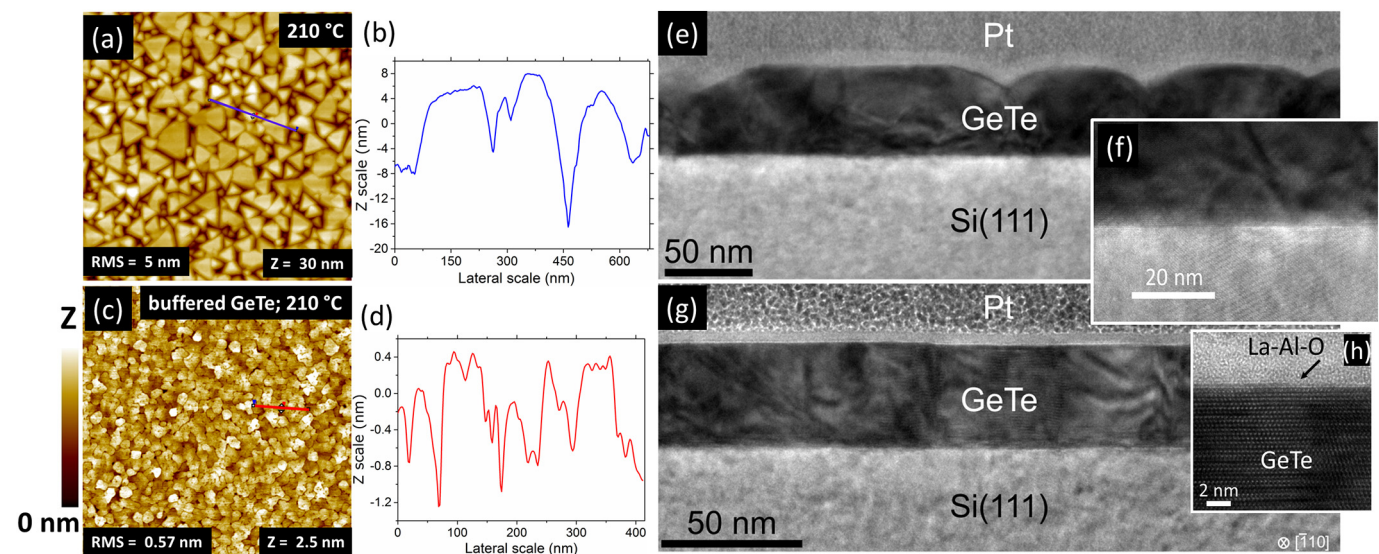


**Fig. 4.** AFM images ( $2 \times 2 \mu\text{m}^2$ ) of a GeTe film deposited at (a)  $210^\circ\text{C}$  on etched Si(111) and (b) its corresponding topographical line profile. (c) shows an AFM image of the GeTe films deposited on a  $\text{Sb}_2\text{Te}_3$ -seeding layer on Si(111) and (d) its corresponding topographical line profile. (e) and (g) represent cross-sectional bright-field TEM images of GeTe thin film deposited on Si(111) and GeTe thin film grown on  $\text{Sb}_2\text{Te}_3$ -buffered Si(111) substrates, respectively. The thin films were deposited at  $210^\circ\text{C}$ . In (e), (f) and (g) the wave-like contrast indicates the strained GeTe lattice of GeTe films. Comparison between both images of (e) and (g) reveals different surface morphologies between the two films. (e) shows a mound-like surface, while (g) and (h) represent a significantly smoother surface. The arrow in (h) marks an atomic step.

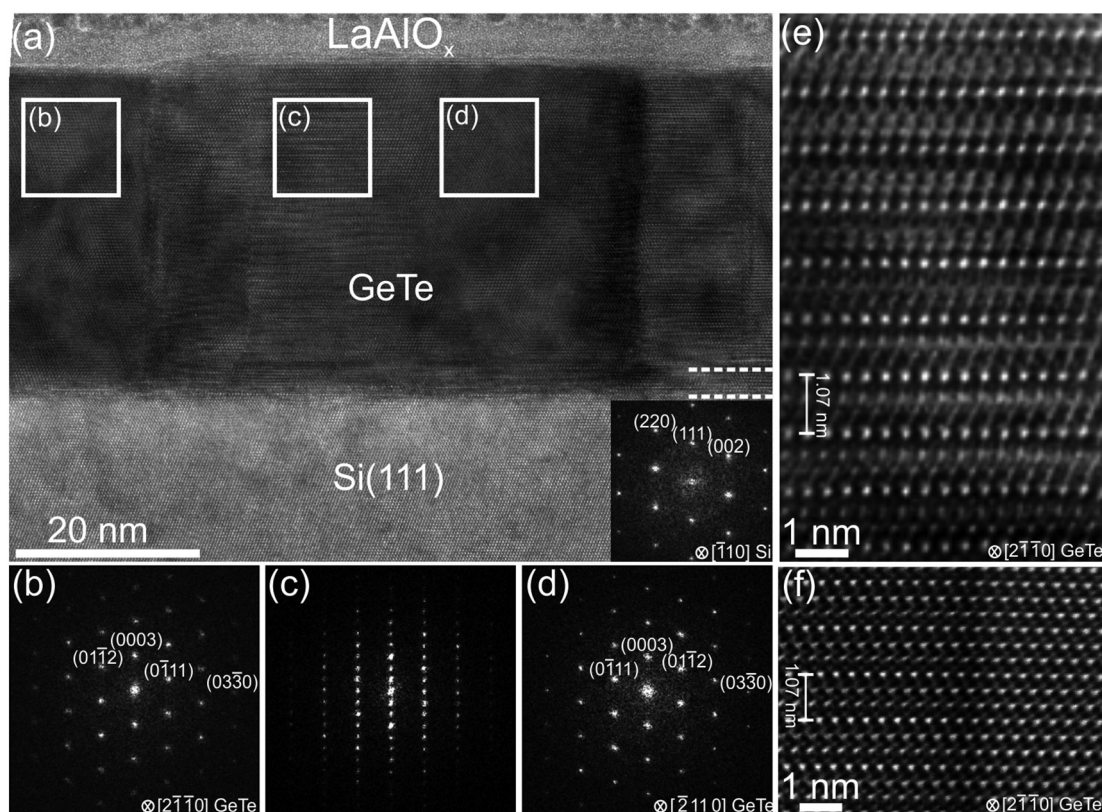


**Fig. 5.** (a) HRTEM image of a GeTe thin film deposited on Sb<sub>2</sub>Te<sub>3</sub>-buffered Si(111) substrate. The two parallel dashed lines adjacent to Si mark the buffer layer. The layer above GeTe is the capping LaAlO<sub>x</sub> amorphous layer. In (a), rectangles marked by b, c and d letters denote the different domains corresponding to different Fast Fourier Transform (FFT) images shown in (b), (c) and (d), respectively. (b) and (d) confirm the presence of {10 $\bar{1}$ 0} twin domains, while the boundary region in (c) shows a more complicated pattern interpreted as an overlap of both crystallites of (b) and (d). (e) and (f) are HRTEM and HAADF-HRSTEM images, respectively, show c-plane stacking in epitaxial GeTe.

transform (FFT) analyses is shown in Fig. 5b, c and d, respectively. The grains with uniform contrast (b and d in Fig. 5a) are neighboring the grains with lamellar fringes contrast (area c in Fig. 5a). The FFT pattern in Fig. 5b and d can be assigned to single grains of GeTe whereas the FFT in Fig. 5c shows extra reflections, e.g. in one-third and two-thirds of the (0003) GeTe reflection. The single grains are rotated by 180° around the c-axis with respect to each other, thus forming two twinned {10 $\bar{1}$ 0} crystallites, while the extra reflections in Fig. 5c are due to a superposition of the twinned domains (see below for a more detailed explanation). Fig. 5e represents a HRTEM image of a GeTe grain with lamellar fringe contrast. The fringes in Fig. 5e are spaced by 1.07 nm, which corresponds to the distance between four Te layers in [0001] direction. Additional investigations by HAADF-HRSTEM revealed the local stacking of Te within those areas (Fig. 5f). Since the image intensity in HAADF micrographs is proportional to the atomic number (Z) as Z<sup>n</sup> (n ≈ 1.7–2.0), the bright dots in the Fig. 5f is, thus, represent Te atomic columns. The intensity of Te columns in the right part of the image is uniform while the intensity of Te columns in the left part of the micrograph is non-uniform, which is due to non-align atomic columns between disordered crystals. In addition, in the left part of Fig. 5f, Te columns spaced by 1.07 nm appeared with higher intensity similar to Fig. 5e.

Based on the TEM and STEM data, a model of GeTe with lamellar fringes contrast can be proposed. Fig. 6a and b show a schematic representation of two parts of {10 $\bar{1}$ 0} GeTe twins. The superposition of these domains in [2 $\bar{1}$ 10] viewing direction resulted in a structure with fringes showing a periodicity of 1.07 nm (Fig. 6c). Fig. 6d represents a side-view of Fig. 6c, where two twinned grains with different thickness (1:2) are neighbors to each other. This results in a lower occupation of Te atoms at double-positioning sites in the proposed model (Fig. 6c). Consequently, GeTe grains with lamellar fringes contrast are overlapped {10 $\bar{1}$ 0} GeTe twinned crystallites in [2 $\bar{1}$ 10] projection. A similar kind of

overlapping twinned grains was also reported for ZnO nanostructures [42]. Fig. 6e and f show simulated HRTEM and HRSTEM images, respectively, which were calculated based on the proposed model in Fig. 6c. A good agreement is found between the simulated and experimental images, confirming reliability of the considered structure model.

#### 4. Conclusions

Epitaxial GeTe thin films were successfully grown on highly lattice mismatched Si(111) and on Sb<sub>2</sub>Te<sub>3</sub>-buffered Si(111) substrates by means of PLD. The epitaxial temperature window is determined to be 210–270 °C for the thin film grown on the unbuffered Si(111) substrates. The in situ investigation using RHEED reveals that the growth of the film was initialized by the formation of an ultra-thin amorphous layer. The films grew according to Stranski-Krastanov growth mode. By employing a 2D bonded Sb<sub>2</sub>Te<sub>3</sub> as a seeding layer on Si(111), the epitaxial temperature window of GeTe can be extended especially towards lower temperatures down to 145 °C. Additionally, the surface topography can be significantly improved with a typical roughness of less than 1 nm, indicating the 2D growth mode of the buffered GeTe film. In both cases, the epitaxial GeTe films were grown with trigonal structure. Moreover, twinned domains were observed in the epitaxial GeTe thin films. The investigation on the local atomic arrangement revealed the presence of overlapped twin domains with characteristic lamellar structure in HRTEM, which is believed to be the characteristic of the alloy. This work demonstrates the possibility of improving the quality of epitaxial thin films of 3D bonded materials by employing a 2D bonded material as a seeding layer. Since improved surface quality of advanced materials is essential for reliability and performance of working devices, this study may pave the way for improving epitaxial growth of any other class of 3D-bonded materials on lattice mismatched substrates

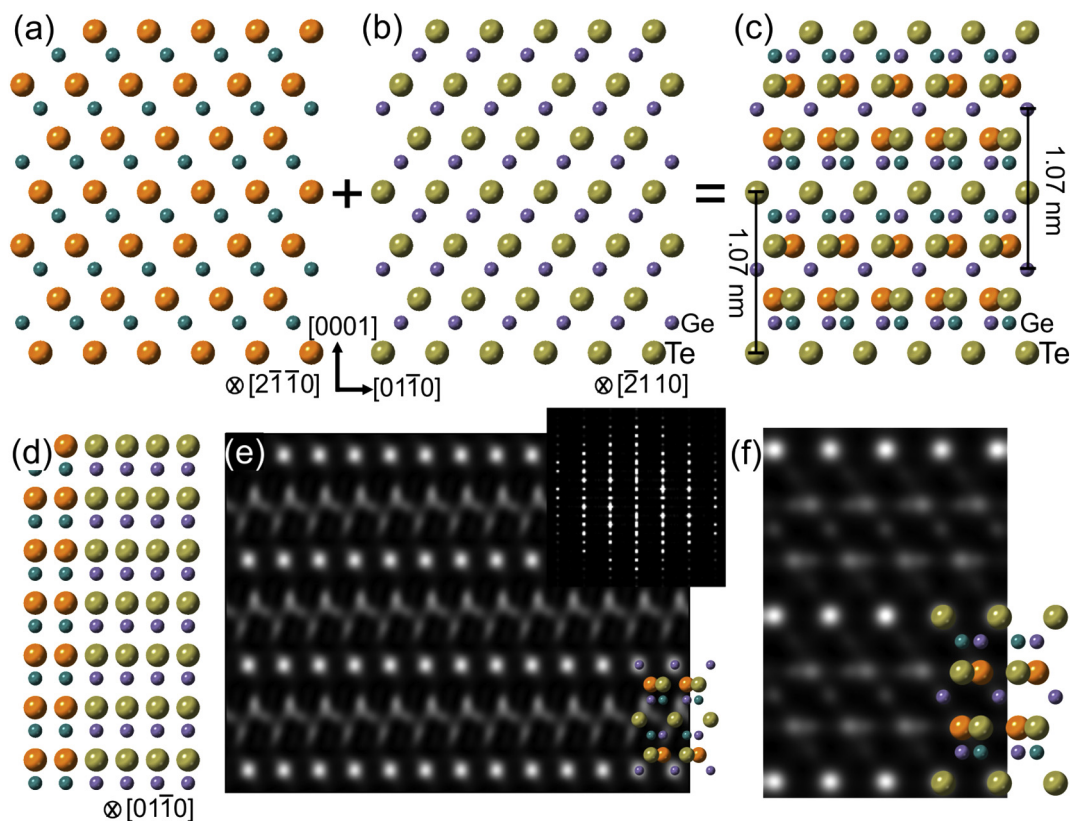


**Fig. 6.** (a) and (b) schematic representation of two parts of 180°-rotated twin domains seen in  $[2\bar{1}\bar{1}0]$  and  $[\bar{2}110]$  directions, respectively. (c) Superimposed structure of (a) and (b), resulting in superposition of twin domains in  $(2\bar{1}\bar{1}0)$ . (d) gives the overlapping twin domain in  $[01\bar{1}0]$  viewing direction. (e) and (f) simulated HRTEM (defocus  $-7$  nm, specimen thickness 32.6 nm) and HAADF-HRSTEM images calculated assuming the model structure shown in (c). The thickness of domain (b) was set to be two times larger as of domain (a). The inset in (e) shows an FFT image. The simulated HRTEM, FFT and HRSTEM images reproduces experimental images in Fig. (c), (e), and (f) well.

by employing 2D-bonded material as seeding layer. Moreover, high-quality surfaces are mandatory for basic research studies e.g. in surface science and for studies on ultrafast phase-transitions in chalcogenide materials [43].

Supplementary data to this article can be found online at <https://doi.org/10.1016/j.matdes.2019.107657>.

#### CRediT authorship contribution statement

**Isom Hilmi:** Data curation, Formal analysis, Investigation, Writing - original draft, Writing - review & editing. **Andriy Lotnyk:** Data curation, Formal analysis, Investigation, Project administration, Supervision, Writing - original draft, Writing - review & editing. **Jürgen W. Gerlach:** Data curation, Formal analysis, Investigation, Writing - original draft, Writing - review & editing. **Philipp Schumacher:** Data curation, Formal analysis, Investigation. **Bernd Rauschenbach:** Project administration, Supervision, Writing - original draft, Writing - review & editing.

#### Acknowledgement

I.H. greatly acknowledges DAAD for the fellowship award. We also thank to A. Mill for TEM sample preparation as well as D. Hirsch for EDX analysis of GeTe sputter target.

#### References

- [1] D. Lencer, M. Salinga, B. Grabowski, T. Hickel, J. Neugebauer, M. Wuttig, A map for phase-change materials, *Nat. Mater.* 7 (2008) 972–977.
- [2] M. Wuttig, N. Yamada, Phase-change materials for rewriteable data storage, *Nat. Mater.* 6 (2007) 824–832.
- [3] K. Shportko, S. Kremers, M. Woda, D. Lencer, J. Robertson, M. Wuttig, Resonant bonding in crystalline phase-change materials, *Nat. Mater.* 7 (2008) 653–658.
- [4] M. Wuttig, V.L. Deringer, X. Gonze, C. Bichara, J.-Y. Raty, Incipient metals: functional materials with a unique bonding mechanism, *Adv. Mater.* 30 (2018), 1803777.
- [5] A. Kolobov, M. Krbal, P. Fons, J. Tominaga, T. Uruga, Distortion-triggered loss of long-range order in solids with bonding energy hierarchy, *Nat. Chem.* 3 (2011) 311–316.
- [6] L. Waldecker, T.A. Miller, M. Rudé, R. Bertoni, J. Osmond, V. Pruneri, R.E. Simpson, R. Ernstorfer, S. Wall, Time-domain separation of optical properties from structural transitions in resonantly bonded materials, *Nat. Mater.* 14 (2015) 991–995.
- [7] T. Chong, L. Shi, R. Zhao, P. Tan, J. Li, H. Lee, X. Miao, A. Du, C. Tung, Phase change random access memory cell with superlattice-like structure, *Appl. Phys. Lett.* 88 (2006), 122114.
- [8] R. Simpson, P. Fons, A. Kolobov, T. Fukaya, M. Krbal, T. Yagi, J. Tominaga, Interfacial phase-change memory, *Nat. Nanotechnol.* 6 (2011) 501–505.
- [9] J.E. Boschker, R. Calarco, Growth of crystalline phase change materials by physical deposition methods, *Adv. Phys.* X2 (2017) 675–694.
- [10] I. Hilmi, A. Lotnyk, J.W. Gerlach, P. Schumacher, B. Rauschenbach, Epitaxial formation of cubic and trigonal Ge-Sb-Te thin films with heterogeneous vacancy structures, *Mater. Des.* 115 (2017) 138–146.
- [11] H. Hardtdegen, S. Rieß, M. Schuck, K. Keller, P. Jost, H. Du, M. Bornhöft, A. Schwedt, G. Mussler, M. v.d. Ahe, J. Mayer, G. Roth, D. Grützmacher, M. Mikulics, A model structure for interfacial phase change memories: epitaxial trigonal  $\text{Ge}_1\text{Sb}_2\text{Te}_4$ , *J. Alloys Compd.* 679 (2016) 285–292.
- [12] I. Hilmi, A. Lotnyk, J.W. Gerlach, P. Schumacher, B. Rauschenbach, Research update: Van-der-Waals epitaxy of layered chalcogenide  $\text{Sb}_2\text{Te}_3$  thin films grown by pulsed laser deposition, *APL Mater.* 5 (2017), 050701.
- [13] M. Kumar, A. Vora-ud, T. Seetawan, J.G. Han, Study of pulsed-DC sputtering induced  $\text{Ge}_2\text{Sb}_2\text{Te}_5$  thin films using facile thermoelectric measurement, *Mater. Des.* 98 (2016) 254–261.
- [14] M. Kumar, A. Vora-ud, T. Seetawan, J.G. Han, Enhancement in thermoelectric properties of cubic  $\text{Ge}_2\text{Sb}_2\text{Te}_5$  thin films by introducing structural disorder, *Energ. Technol.* 4 (2016) 375–379.
- [15] M. Kumar, A. Vora-ud, T. Seetawan, J.G. Han, Thermoelectric power factor enhancement by pulsed plasma engineering in magnetron sputtering induced  $\text{Ge}_2\text{Sb}_2\text{Te}_5$  thin films, *ACS Appl. Energy Mater.* 1 (2018) 4025–4031.
- [16] T.L. Anderson, H.B. Krause, Refinement of the  $\text{Sb}_2\text{Te}_3$  and  $\text{Sb}_2\text{Te}_2\text{Se}$  structures and their relationship to nonstoichiometric  $\text{Sb}_2\text{Te}_{3-y}\text{Se}_y$  compounds, *Acta Crystallogr. B* 30 (1974) 1307–1310.
- [17] A. Koma, Van der Waals epitaxy—a new epitaxial growth method for a highly lattice-mismatched system, *Thin Solid Films* 216 (1992) 72–76.
- [18] P.B. Pereira, I. Sergueev, S. Gorsse, J. Dadda, E. Müller, R.P. Hermann, Lattice dynamics and structure of GeTe, SnTe and PbTe, *Phys. Status Solidi B* 250 (2013) 1300–1307.

- [19] L. Shelimova, O. Karpinskii, E. Avilov, M. Kretova, Crystal structure, phase transitions, and mechanical properties of GeTe-based solid solutions in the GeTe-PbTe-MTe systems ( $M = \text{Mn, Sc, La}$ ), *Inorg. Mater.* 29 (1993) 1291–1298.
- [20] T. Chattopadhyay, J. Boucherle, Neutron diffraction study on the structural phase transition in GeTe, *J. Phys. C Solid State Phys.* 20 (1987) 1431–1440.
- [21] T. Nonaka, G. Ohbayashi, Y. Toriumi, Y. Mori, H. Hashimoto, Crystal structure of GeTe and  $\text{Ge}_2\text{Sb}_2\text{Te}_5$  meta-stable phase, *Thin Solid Films* 370 (2000) 258–261.
- [22] J.L. Da Silva, A. Walsh, H. Lee, Insights into the structure of the stable and metastable  $(\text{GeTe})_m(\text{Sb}_2\text{Te}_3)_n$  compounds, *Phys. Rev. B* 78 (2008), 224111.
- [23] K. Perumal, Epitaxial Growth of Ge-Sb-Te Based Phase Change Materials, Humboldt-Universität Zu Berlin, 2013 (Mathematisch-Naturwissenschaftliche Fakultät I).
- [24] A. Giussani, K. Perumal, M. Hanke, P. Rodenbach, H. Riechert, R. Calarco, On the epitaxy of germanium telluride thin films on silicon substrates, *Phys. Status Solidi B* 249 (2012) 1939–1944.
- [25] G. Wang, X. Zhu, J. Wen, X. Chen, K. He, L. Wang, X. Ma, Y. Liu, X. Dai, Z. Fang, Atomically smooth ultrathin films of topological insulator  $\text{Sb}_2\text{Te}_3$ , *Nano Res.* 3 (2010) 874–880.
- [26] D. Bang, H. Awano, J. Tominaga, A.V. Kolobov, P. Fons, Y. Saito, K. Makino, T. Nakano, M. Hase, Y. Takagaki, Mirror-symmetric magneto-optical Kerr rotation using visible light in  $[(\text{GeTe})_2(\text{Sb}_2\text{Te}_3)_1]_n$  topological superlattices, *Sci. Rep.* 4 (2014) 5727.
- [27] A. Lotnyk, I. Hilmi, U. Ross, B. Rauschenbach, Van der Waals interfacial bonding and intermixing in GeTe- $\text{Sb}_2\text{Te}_3$ -based superlattices, *Nano Res.* 11 (2018) 1676–1686.
- [28] J. Momand, R. Wang, J.E. Boschker, M.A. Verheijen, R. Calarco, B.J. Kooi, Interface formation of two- and three-dimensionally bonded materials in the case of GeTe- $\text{Sb}_2\text{Te}_3$  superlattices, *Nanoscale* 7 (2015) 19136–19143.
- [29] P. Kowalczyk, F. Hippert, N. Bernier, C. Mocuta, C. Sabbione, W. Batista-Pessoa, P. Noé, Impact of stoichiometry on the structure of van der Waals layered GeTe/ $\text{Sb}_2\text{Te}_3$  Superlattices used in interfacial phase-change memory (iPCM) devices, *Small* 14 (2018), 1704514.
- [30] A. Lotnyk, D. Poppitz, U. Ross, J. Gerlach, F. Frost, S. Bernütz, E. Thelander, B. Rauschenbach, Focused high- and low-energy ion milling for TEM specimen preparation, *Microelectron. Reliab.* 55 (2015) 2119–2125.
- [31] P. Stadelmann, EMS—a software package for electron diffraction analysis and HREM image simulation in materials science, *Ultramicroscopy* 21 (1987) 131–145.
- [32] J. Barthel, Dr. Probe: a software for high-resolution STEM image simulation, *Ultramicroscopy* 193 (2018) 1–11.
- [33] CaRIne Crystallography Divergent S. A., <http://carine.crystallography.pagespro-orange.fr>.
- [34] R. Wang, W. Zhang, J. Momand, I. Ronneberger, J.E. Boschker, R. Mazzarello, B.J. Kooi, H. Riechert, M. Wuttig, R. Calarco, Formation of resonant bonding during growth of ultrathin GeTe films, *NPG Asia Mater.* 9 (2017) e396.
- [35] I.N. Stranski, L. Krastanow, Zur Theorie der orientierten Ausscheidung von Ionenkristallen aufeinander, *Monatsh. Chem.* 71 (1937) 351–364.
- [36] U. Ross, A. Lotnyk, E. Thelander, B. Rauschenbach, Microstructure evolution in pulsed laser deposited epitaxial Ge-Sb-Te chalcogenide thin films, *J. Alloys Compd.* 676 (2016) 582–590.
- [37] R. Wang, J.E. Boschker, E. Bruyer, D.D. Sante, S. Picozzi, K. Perumal, A. Giussani, H. Riechert, R. Calarco, Toward truly single crystalline GeTe films: the relevance of the substrate surface, *J. Phys. Chem. C* 118 (2014) 29724–29730.
- [38] G.-F. Zhou, B.A. Jacobs, High performance media for phase change optical recording, *Jpn. J. Appl. Phys.* 38 (1999) 1625–1628.
- [39] Y. Saito, P. Fons, A.V. Kolobov, J. Tominaga, Self-organized van der Waals epitaxy of layered chalcogenide structures, *Phys. Status Solidi B* 252 (2015) 2151–2158.
- [40] R. Simpson, P. Fons, A. Kolobov, M. Krbal, J. Tominaga, Enhanced crystallization of GeTe from an  $\text{Sb}_2\text{Te}_3$  template, *Appl. Phys. Lett.* 100 (2012) 021911.
- [41] X. Zhou, J. Kalikka, X. Ji, L. Wu, Z. Song, R.E. Simpson, Phase-change memory materials by design: a strain engineering approach, *Adv. Mater.* 28 (2016) 3007–3016.
- [42] V. Hrkac, L. Kienle, S. Kaps, A. Lotnyk, Y.K. Mishra, U. Schuermann, V. Duppel, B.V. Lotsch, R. Adelung, Superposition twinning supported by texture in ZnO nanospikes, *J. Appl. Crystallogr.* 46 (2013) 396–403.
- [43] M. Behrens, A. Lotnyk, J.W. Gerlach, I. Hilmi, T. Abel, P. Lorenz, B. Rauschenbach, Ultrafast interfacial transformation from 2D-to 3D-bonded structures in layered Ge-Sb-Te thin films and heterostructures, *Nanoscale* 10 (2018) 22946–22953.